Flexible long-range surface plasmon polariton single-mode waveguide for optical interconnects

Christian Vernoux, Yiting Chen, Laurent Markey, Cosmin Spârchez, Juan Arocas, Thorsten Felder, Marcel Neitz, Lars Brusberg, Jean-Claude Weeber, Sergey Bozhevolnyi, et al.

Flexible long-range surface plasmon polariton single-mode waveguide for optical interconnects

Vernoux, Christian; Chen, Yiting; Markey, Laurent; Spârchez, Cosmin; Arocas, Juan; Felder, Thorsten; Neitz, Marcel; Brusberg, Lars; Weeber, Jean Claude; Bozhevolnyi, Sergey I.; Dereux, Alain

Published in:
Optical Materials Express

DOI:
10.1364/OME.8.000469

Publication date:
2018

Document version:
Final published version

Document license:
CC BY

Citation for pulished version (APA):
Vernoux, C., Chen, Y., Markey, L., Spârchez, C., Arocas, J., Felder, T., Neitz, M., Brusberg, L., Weeber, J. C., Bozhevolnyi, S. I., & Dereux, A. (2018). Flexible long-range surface plasmon polariton single-mode waveguide for optical interconnects. *Optical Materials Express*, *8*(2), 469-484. https://doi.org/10.1364/OME.8.000469

Research Article | Vol. 8, No. 2 | 1 Feb 2018 | OPTICAL MATERIALS EXPRESS 469
Optical Materials EXPRESS

Flexible long-range surface plasmon polariton single-mode waveguide for optical interconnects

CHRISTIAN VERNOUX,[1] YITING CHEN,[2] LAURENT MARKEY,[1,*] COSMIN SPÂRCHEZ,[1] JUAN AROCAS,[1] THORSTEN FELDER,[3], MARCEL NEITZ,[4] LARS BRUSBERG,[5] JEAN-CLAUDE WEEBER,[1] SERGEY I. BOZHEVOLNYI,[2] AND ALAIN DEREUX[1]

[1]*Laboratoire Interdisciplinaire Carnot de Bourgogne, UMR 6303 CNRS–Université de Bourgogne Franche-Comté, 21078 Dijon, France*
[2]*Centre for Nano Optics, University of Southern Denmark, Campusvej 55, DK-5230 Odense M, Denmark*
[3]*Momentive Performance Materials GmbH, Chempark Leverkusen, 51368 Leverkusen, Germany*
[4]*Technische Universität Berlin, Gustav-Meyer-Allee 25, 13355 Berlin, Germany*
[5]*Fraunhofer Institute for Reliability and Microintegration, Gustav-Meyer-Allee 25, 13355 Berlin, Germany*
**laurent.markey@u-bourgogne.fr*

Abstract: We present the design, fabrication and characterization of long-range surface plasmon polariton waveguide arrays with materials, mainly silicones, carefully selected with the aim to be used as mechanically flexible single-mode optical interconnections, the so-called "plasmonic arc" working at 1.55µm. The fabricated plasmonic arcs show a TM/TE polarization ratio of ~25 dB. By using the cut-back method, the straight propagation loss at 1.55µm is estimated to 0.5-1 dB/mm and coupling loss to ~1-2 dB/facet after dicing. In the free-standing S-curved configuration, the bending loss of single cladding plasmonic arc is 2.2-2.8 dB/90° at bending radius 2.5 mm. For double cladding plasmonic arcs, it is decreased to 0.7-1.7 dB/90° for the same radius. The coupling loss with single-mode glass PCB waveguides is estimated to be 1.7 dB/interface in the best condition.

OCIS codes: (230.7370) Waveguides; (250.5403) Plasmonics; (200.4650) Optical interconnects; (310.1860) Deposition and fabrication; (160.4670) Optical materials; (130.5460) Polymer waveguides.

References and links

1. W. L. Barnes, A. Dereux, and T. W. Ebbesen, "Surface plasmon subwavelength optics," Nature **424**(6950), 824–830 (2003).
2. R. Charbonneau, P. Berini, E. Berolo, and E. Lisicka-Shrzek, "Experimental observation of plasmon polariton waves supported by a thin metal film of finite width," Opt. Lett. **25**(11), 844–846 (2000).
3. P. Berini, "Long-range surface plasmon polaritons," Adv. Opt. Photonics **1**(3), 484–588 (2009).
4. S. I. Bozhevolnyi, *Plasmonic: Nanoguides and Circuits* (World Scientific Pub, 2009).
5. D. K. Gramotnev and S. I. Bozhevolnyi, "Plasmonics beyond the diffraction limit," Nat. Photonics **4**(2), 83–91 (2010).
6. D. Kalavrouziotis, S. Papaioannou, G. Giannoulis, D. Apostolopoulos, K. Hassan, L. Markey, J.-C. Weeber, A. Dereux, A. Kumar, S. I. Bozhevolnyi, M. Baus, M. Karl, T. Tekin, O. Tsilipakos, A. Pitilakis, E. E. Kriezis, H. Avramopoulos, K. Vyrsokinos, and N. Pleros, "0.48Tb/s (12x40Gb/s) WDM transmission and high-quality thermo-optic switching in dielectric loaded plasmonics," Opt. Express **20**(7), 7655–7662 (2012).
7. C. Haffner, W. Heni, Y. Fedoryshyn, J. Niegemann, A. Melikyan, D. L. Elder, B. Baeuerle, Y. Salamin, A. Josten, U. Koch, C. Hoessbacher, F. Ducry, L. Juchli, A. Emboras, D. Hillerkuss, M. Kohl, L. R. Dalton, C. Hafner, and J. Leuthold, "All-plasmonic Mach–Zehnder modulator enabling optical high- speed communication at the microscale," Nat. Photonics **9**(8), 525–528 (2015).
8. T. Nikolajsen, K. Leosson, and S. I. Bozhevolnyi, "In-line extinction modulator based on long-range surface plasmon polaritons," Opt. Commun. **244**(1–6), 455–459 (2005).

#313558 https://doi.org/10.1364/OME.8.000469
Journal © 2018 Received 15 Nov 2017; revised 19 Jan 2018; accepted 19 Jan 2018; published 29 Jan 2018

Optical Materials EXPRESS

9. J. T. Kim, K. H. Chung, and C. G. Choi, "Thermo-optic mode extinction modulator based on graphene plasmonic waveguide," Opt. Express **21**(13), 15280–15286 (2013).
10. R. Dangel, J. Hofrichter, F. Horst, D. Jubin, A. La Porta, N. Meier, I. M. Soganci, J. Weiss, and B. J. Offrein, "Polymer waveguides for electro-optical integration in data centers and high-performance computers," Opt. Express **23**(4), 4736–4750 (2015).
11. M. A. Taubenblatt, "Optical Interconnects for High-Performance Computing," J. Lightwave Technol. **30**(4), 448–457 (2012).
12. S. I. Bozhevolnyi, V. S. Volkov, K. Leosson, and A. Boltasseva, "Surface Plasmon polariton waveguiding in random surface nanostructures," J. Microsc. **209**(Pt 3), 209–213 (2003).
13. A. Degiron, S.-Y. Cho, C. Harrison, N. M. Jokerst, C. Dellagiacoma, O. Martin, and D. R. Smith, "Experimental comparison between conventional and hybrid long-range surface plasmon waveguide bends," Phys. Rev. A **77**(2), 021804 (2008).
14. J. T. Kim, S. Park, J. J. Ju, S. K. Park, M.-S. Kim, and M.-H. Lee, "Low-Loss Polymer-Based Long-Range Surface Plasmon-Polariton Waveguide," IEEE Phot. Tech. Letters **19**(18), 1374–1376 (2007).
15. J.-M. Lee, S. Park, M.-S. Kim, S. K. Park, J. T. Kim, J.-S. Choe, W.-J. Lee, M.-H. Lee, and J. J. Ju, "Low Bending Loss Metal Waveguide Embedded in a Free-Standing Multilayered Polymer Film," Opt. Express **17**(1), 228–234 (2009).
16. S. Park, J. J. Ju, J. T. Kim, M.-S. Kim, S. K. Park, J.-M. Lee, W.-J. Lee, and M.-H. Lee, "Sub-dB/cm propagation loss in silver stripe waveguides," Opt. Express **17**(2), 697–702 (2009).
17. J. T. Kim, S. Park, S. K. Park, M.-S. Kim, M.-H. Lee, and J. J. Ju, "Gold stripe optical waveguides fabricated by a novel double-layered liftoff process," ETRI J. **31**(6), 778–783 (2009).
18. J. T. Kim, J. J. Ju, S. Park, M.-S. Kim, S. K. Park, and S. Y. Shin, "Hybrid plasmonic waveguide for low-loss lightwave guiding," Opt. Express **18**(3), 2808–2813 (2010).
19. J. T. Kim, S. Park, J. J. Ju, S. Lee, and S. Kim, "Low bending loss characteristics of hybrid plasmonic waveguide for flexible optical interconnect," Opt. Express **18**(23), 24213–24220 (2010).
20. J. T. Kim, J. J. Ju, S. Park, M.-S. Kim, S. K. Park, and M.-H. Lee, "Chip-to-chip optical interconnect using gold long-range surface plasmon polariton waveguides," Opt. Express **16**(17), 13133–13138 (2008).
21. M. Walther, D. G. Cooke, C. Sherstan, M. Hajar, M. R. Freeman, and F. Hegmann, "Terahertz conductivity of thin gold films at the metal-insulator percolation transition," Phys. Rev. B **76**(12), 1–9 (2007).
22. I. Slovinsky, G. K. Stefansson, A. Kossoy, and K. Leosson, "Propagation loss of long-range surface plasmon polariton gold stripe waveguides in the thin-film limit," Plasmonics **8**(4), 1613–1619 (2013).
23. J. Guo and R. Adato, "Extended long range plasmon waves in finite thickness metal film and layered dielectric materials," Opt. Express **14**(25), 12409–12418 (2006).
24. C. G. Durfee, T. E. Furtak, R. T. Collins, and R. E. Hollingsworth, "Metal-oxide-semiconductor-compatible ultra-long-range surface plasmon modes," J. Appl. Phys. **103**(11), 113106 (2008).
25. H. Ma, A. K.-Y. Jen, and L. R. Dalton, "Polymer-Based Optical Waveguides: Materials, Processing, and Devices," Adv. Mater. **14**(19), 1339–1365 (2002).
26. S. K. Park, J.-M. Lee, S. Park, J. T. Kim, M.-S. Kim, M.-H. Lee, and J. J. Ju, "Highly fluorinated and photocrosslinkable liquid prepolymers for flexible optical waveguides," J. Mater. Chem. **21**(6), 1755–1761 (2011).
27. A. Elmogi, E. Bosman, J. Missinne, and G. Van Steenberge, "Comparison of epoxy- and siloxane-based single-mode optical waveguides defined by direct-write lithography," Opt. Mater. **52**, 26–31 (2016).
28. ChemOptics website, http://www.chemoptics.co.kr/eng/main/main.php.
29. B. L. Booth, J. E. Marchegiano, C. T. Chang, R. J. Furmanak, D. M. Graham, and R. G. Wagner, "Polyguide polymeric technology for optical interconnect circuits and components," Proc. SPIE **3005**, 238–253 (1997).
30. M. U. Khan, J. Justice, J. Petäjä, T. Korhonen, A. Boersma, S. Wiegersma, M. Karppinen, and B. Corbett, "Multi-level single mode 2D polymer waveguide optical interconnects using nano-imprint lithography," Opt. Express **23**(11), 14630–14639 (2015).
31. R. Buestrich, F. Kahlenberg, M. Popall, P. Dannberg, R. Müller-Fiedler, and O. Rösch, "ORMOCERs for Optical Interconnection Technology," J. Sol-Gel Sci. Technol. **20**(2), 181–186 (2001).
32. W. H. Wong, J. Zhou, and E. Y. B. Pun, "Low-loss polymeric optical waveguides using electron-beam direct writing," Appl. Phys. Lett. **78**(15), 2110–2112 (2001).
33. T. Nikolajsen, K. Leosson, I. Salakhutdinov, and S. I. Bozhevolnyi, "Polymer-based surface-plasmon-polariton stripe waveguides at telecommunication wavelengths," Appl. Phys. Lett. **82**(5), 668–670 (2003).
34. S. Park, M.-S. Kim, J. T. Kim, S. K. Park, J. J. Ju, and M.-H. Lee, "Long range surface plasmon polariton waveguides at 1.31 and 1.55 μm wavelengths," Opt. Commun. **281**(8), 2057–2061 (2008).
35. D. K. Cai, A. Neyer, R. Kuckuk, and H. M. Heise, "Optical absorption in transparent PDMS materials applied for multimode waveguides fabrication," Opt. Mater. **30**(7), 1157–1161 (2008).
36. M. P. Nezhad, S. Zamek, L. Pang, and Y. Fainman, "Fabrication approaches for metallo-dielectric plasmonic waveguides," in Advanced Fabrication Technologies for Micro/Nano Optics and Photonics, Proc. SPIE **6883**, 68830S (2008).
37. B. Chan, H. Lin, C. Carver, J. Huang, and J. Berry, "Organic Optical Waveguide Fabrication in a Manufacturing Environment" in *Electronic Components and Technology Conference* (ECTC), Proceedings 60th (IEEE, 2010)
38. C. De Bernardi, A. Küng, and O. Leminger, in *Photonic Devices for Telecommunications*, Guekos, ed. (Springer, 1999), pp 127–128.

Optical Materials EXPRESS

39. L. Brusberg, H. Schröder, M. Queisser, and K.-D. Lang, "Single-mode Glass Waveguide Platform for DWDM Chip-to-Chip Interconnects" in Proceedings of IEEE 62nd Electronic Components and Technology Conference (ECTC), (IEEE 2012).
40. L. Brusberg, M. Neitz, and H. Schröder, "Single-mode glass waveguide technology for optical interchip communication on board level," in Proc. SPIE **8267**, Optoelectronic Interconnects **XII**, 82670M (2012).

1. Introduction

Plasmonics offer a great potential in the field photonic integrated circuits [1] and propose a large variety of structures for passive or active functionalities. In this work, the long-range surface plasmon polariton waveguide (LRSPPW) is developed with the aim to offer a transmission line interfacing chips and boards in data centers or high performance computers (HPC) applications, where lower power consumption, higher speed and lower cost technologies are needed. The LRSPPW concept invented in the early 80s [2,3] has been demonstrated with different polymers as the dielectric cladding material. A review on LRSPP has been published by Berini [3]. They do not offer so tight confinement of the electric field as some other types of plasmonic waveguide, but for sufficiently thin metal, the losses are reduced dramatically, showing propagation lengths in the millimeter range [4]. Conveniently, the LRSPP mode can be excited directly by end-fire coupling and the field distribution can be adjusted to that of a single-mode fiber by varying the strip width and thickness. The pitch of the LRSPPW arrays can reach 100µm or less. This attractive feature promotes their application in integrated optical devices and interconnects with a high density of channels to be interconnected with arrays of VCSELs or photodiodes. Another remarkable advantage of plasmonics is that the metal supporting the surface plasmon can also serve as electric wiring in parallel with its optical waveguide function, leading to the demonstration of active plasmonic devices like modulators and interferometers [5–7]. In this respect thermo-optic in-line extinction modulator based on LRSPPW have been demonstrated [8,9].

To be able to realize short-distance single-mode interconnectors in optical boards, for example chip-to-chip or chip-to-board interfaces in narrow spaces, a mechanically flexible, shapeable waveguide technology is a very attractive approach which is currently addressed by polymer waveguides [10,11]. Provided that they could reach the same level of optical loss, LRSPPW could offer an interesting alternative to polymer waveguides and not only for passive devices. Different kinds of bend configuration of LRSPPWs have been experimented, either in-plane [12,13] or out-of-plane bend, implying a flexible characteristic of the waveguides. Flexible self-supported free-standing LRSPPW have been developed experimentally by a research group in Korea [14–19] and they demonstrated their capability for chip-to-chip interconnection between VCSEL and photodiode at $\lambda = 1.3$ µm [20]. Here we designate them as "plasmonic arcs". In this work we examine the potential of several commercial polymer materials to make a stable, resistant, flexible, free-standing plasmonic arc operating as single-mode interconnect at 1550 nm telecom wavelength, a wavelength at which polymers generally have much higher absorption. We develop a fabrication method based on the plasma etching of a gold film with a lithography mask. We fabricate 100µm pitch plasmonic arc arrays made with two selected materials and study their propagation loss and bending loss at 1550 nm. Finally we measure coupling loss with glass waveguide which are used as optical printed circuit board (OPCB) components.

2. Design

The simplest LRSPPW has a single-cladding structure (shown in Fig. 1(a)) consisting of a very thin metal strip (width w, thickness t) embedded in a dielectric medium of uniform refractive index. As the electric field is strongly attenuated in the metal, with sufficiently thin metal, most of the energy of the mode will propagate in the lossless surrounding dielectric (Fig. 1(b)), thus leading to a low propagation loss. The metal used throughout this study was gold, usually preferred over silver for its long-term environmental stability. In our design, the

Optical Materials EXPRESS

thickness of gold strip is 15 nm, which ensures both good confinement of the electric field and desirable propagation length.

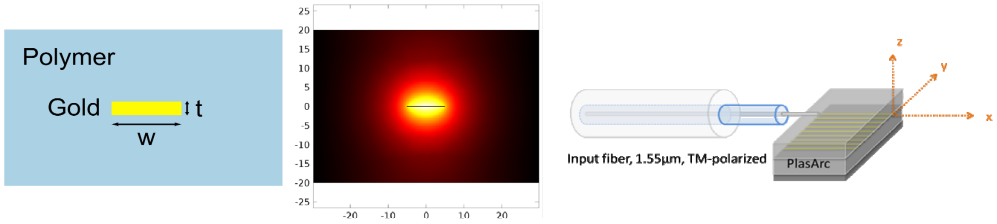

Fig. 1. Single-cladding LRSPPW configuration. (a) Schematic structure. (b) Electric field distribution of the fundamental TM mode. (c) Representation of the LRSPPW coupled with SM-fiber. Samples contain arrays of identical waveguides with 100µm pitch.

The propagation loss of SPPs can be effectively reduced by decreasing the thickness of the gold strip, due to reduced ohmic loss in the metal [3]. However, in practice metal layers with thickness lower than ~15 nm are less homogeneous, approaching the percolation limit of the film [21]. There are many channels of losses other than the fundamental absorption of the metal, and in particular scattering losses from imperfect edges and surface roughness of the metal strip. This makes the actual propagation loss higher than expected from simulation for very thin metal strips [22]. In addition, a minimum thickness limit is preferred in practice to obtain acceptable thickness control with the quartz crystal microbalance used for the measurement. The actual thickness was in the 15-20 nm range throughout the experiments

Beyond the single cladding configuration, more advanced structures have been proposed to improve the performance, in particular the multilayer and dual-core structures [15,18,19,23], which were introduced to obtain lower out-of-plane bending loss than the single cladding one. Other types of structures have been proposed (not represented here) comprising asymmetric structures where a thin dielectric layer deposited on one side of the metal is expected to increase the propagation length [24].

3. Material selection for the flexible claddings

To make the plasmonic arc at low cost, bendable polymer materials were selected on the basis of various criteria, such as mechanical performance, environmental stability, processability and optical properties in the telecom wavelength range. The material should form smooth films in the thickness range of micrometers to tens of micrometers and be compatible with the processes and chemicals utilized in the microfabrication steps (lithography, etching, lift-off) of the metal strip, with a particular care on the adhesion at the metal - polymer interfaces, to avoid the introduction of any gap due to the low adherence energy of gold. Its refractive index should also be tunable to realize multiple-layer configurations, where a $\Delta n/n$ in the range 0.1–1% is needed. In addition, the materials used for the different layers of these configurations should be matched in terms of strain susceptibility under bending.

Polymer materials used in waveguide fabrication include different families: polystyrenes, polycarbonates, polyacrylates, polyimides, epoxy resins, silicones (siloxanes), sol-gels, inorganic/organic hybrids like ormocer and many other specific polymer materials, very often integrating fluorine substituents for higher transparency at telecom wavelengths. In our case, all the requirements qualify transparent elastomers like silicones (polysiloxanes) as excellent candidates. To assure stability a high degree of cross-linking of the polymer is desired. It is realized either by thermal cure or UV cure, or both. Table 1 lists a few available polymer materials commonly used for the fabrication of waveguides at 1.55 µm and at the end of the table the three materials tested in this work, where the materials provided by Momentive are research grades, thus a composition under development. Many other optical polymers of potential interest have been reported in the literature [25,26]. Elastic modulus values found in the literature and often coming from tensile loading tests can be compared for a prime and

Optical Materials EXPRESS

simple evaluation of flexibility. They range from a few thousand MPa for common polymers like PMMA, SU-8 or BCB, to 0.3-0.9 MPa for an elastomer like PDMS. In order to get good flexibility down to 1-2 mm radius of curvature with limited internal stress of the film, we estimate that the modulus should not exceed a few tens of MPa. Some materials like Ormocer can have this modulus varied over several decades depending on specific formulation conditions. In the fourth column of Table 1, we give a rough assessment of flexibility based on our experiments. The refractive index at 1.55 µm is also listed, based on either literature or manufacturer data. The ranged values in the table reflect the possibility of adjusting the refractive index as most of the materials listed are supplied in different grades of index, and these can be blended to allow for a controlled index tuning. Very few data can be found for the imaginary part k or material's absorption coefficient. The materials we have tested have very low absorption and k was neglected in our computations. The literature's best propagation loss values of respectively polymer waveguides and LRSPPW summarized in the table allow us to make a comparison between the purely photonic and the plasmonic waveguides for the same 1.55µm excitation and single-mode condition. Most often a dramatic increase of the propagation loss is observed when the wavelength changes from 1.31 to 1.55 µm, like for example with EpoCore: 0.49 and 2.23 dB/cm respectively at 1.31 and 1.55 µm [27]. This is most probably due to higher absorption of many polymers at 1.55 µm.

Table 1. Possible commercial materials and important parameters for the flexible plasmonic Arc. Colored blocks refer to the results obtained in this work.

Material	Polymer type	Thermal stability (°C)	Flexibility and integrity of ~20-40µm film	n at 1.55 µm	Loss in dB/cm at λ = 1.55µm	
					Single-mode polymer waveguide	LRSPPW
PMMA	acrylate	85	low	1.49	0.6 [29]	-
SU-8	epoxy novolak	>200	low	1.57	0.48 [32]	5
BCB	benzocyclobutene	350	low	1.535	1.5 [25]	6 - 8 [33]
PDMS	siloxane	>250	high	1.396	-	-
ORMOCER	organic/inorganic hybrid silicone	270	medium	1.52—1.538 from [31]	0.75 – 0.8 [30,31]	-
EPO CORE/CLAD	epoxy	230	-	1.575 / 1.563	2.23 [27]	-
Exguide ZPU / LFR	fluorinated acrylate	300 [28]	-	1.43 / 1.46	0.35 [14]	1.4 [34]
Exguide FOWG	acrylate –co-ethylene oxide	280	high	1.506—1.547	-	32
LIGHTLINK	silsesquioxane	high	high	1.473	1.36 [27]	3 – 10
MPM526A&B	epoxy	200	high	1.41—1.47	-	5 – 12

The acrylate family declined for wave-guiding is rich and halogenated acrylate can provide losses as low as 0.2 dB/cm at 1.55 µm for photonic waveguides and be made environmentally stable [25]. ZPU12 and ZPU13 are fluorinated acrylate UV-curable epoxy resins from company Chemoptics; they have been used to produce LRSPPW [34] and photonic polymer waveguide [14] which both exhibit low propagation loss at 1.55 µm (1.4 and 0.35 dB/cm respectively). SU-8 and BCB have the disadvantage of having limited flexibility, with their elasticity modulus lying in the 2-5 GPa range. In addition, their absorption loss at 1.55 µm is relatively high compared to other polymers due to absorption bands in this range with a k value estimated to ~$1e^{-5}$ at 1.55 µm for cross-linked SU-8.

Optical Materials EXPRESS

Nevertheless we fabricated LRSPPW with SU-8 and have measured a ~5 dB/cm propagation loss. Ormocer or Epocore / Epoclad could be interesting choices but their film flexibility has to be investigated. PDMS is also an option with report of the propagation loss of ~0.027 dB/cm for its multimode photonic waveguides at 850 nm, but PDMS possesses an absorption band at ~1500 nm which reduces its potential at telecom wavelength [35] with a k value estimated to be ~0.07. In addition problems of poor adhesion with gold have been reported for this material, as well as problems of compatibility with the lithography process used for producing the metal waveguides [36]. Exguide FOWG from Korean company Chemoptics is an ethylene-oxide and acrylate based copolymer including fluorinated styrene groups. It has excellent elastomeric properties and thermal stability (stable up to 270°C), and was our initial choice because of the excellent performances reported for plasmonic arcs operated at 1.31µm, in particular a propagation loss below 1 dB/cm [18] and low bending losses [15,19]. We remark that no loss data can be found in the literature for FOWG-based LRSPPW at 1.55µm. It is also noticeable that FOWG was preferred over ZPU for bending studies. We tested a fabrication method for FOWG based on the indications this group has published (see section 4 below). In conclusion, among the polymers listed, we select the last three as the most suitable for flexible plasmonic arc interconnects applications.

We fabricated FOWG films with material grades FOWG-115 and 116 using the following procedure. Before spin-coating it was found necessary to use an adhesion promoter to get a correct wetting of a Si wafer. After spin-coating, cross-linking is achieved by UV-curing under inert atmosphere. The films are exposed for at least 20 min to the diffusive light of a UV lamp in an argon purged glove box. It was found difficult to produce correctly cured, smooth and robust film if all these specific conditions were not respected.

Lightlink possesses a silsesquioxane backbone. It has been used to produce photonic polymer waveguides with a loss of 0.05 dB/cm at λ = 850 nm [37]. It is now commercially available in different grades, either thermal cure or UV cure from Microchem. In this work Lightlink films were made with grade XH-100145 which was chosen for its simpler thermal cure process. Lightlink films are easily formed by spin coating (1500 rpm for 5 µm thickness) and 90 °C + 160 °C baking steps. Multiple layers can be added on top of each other following the same process in order to reach the desired cladding thickness.

Momentive Performance Materials GmbH (Germany) provided two grades of research materials MPM526A&B allowing tuning the refractive index of the material blend. The blend could be cured by UV irradiation + a thermal treatment. Nice homogeneous and resistant flexible films were obtained. The thickness ranges were different for the prepared material compositions. To obtain the desired thicknesses, the spin–coating spin speed was adjusted and in the cases where a single coating was too thin, double layers of the same were realized.

4. Plasmonic arc fabrication

For Lightlink or MPM526A&B, we developed a fabrication method for plasmonic arcs based on optical lithography and plasma etching of gold. The cured films made of those two materials were able to withstand etching without being affected too strongly, contrary to Chemoptics's FOWG, composed of ethylene-oxide and acrylate copolymers. The initial FOWG film quality was lost after etching, hindering the finalization of the waveguides. The siloxane nature, with the presence of the heavier Si atoms in Lightlink and in the MPM526A&B blends used is the most probable explanation of this difference of etching behavior. In the case of FOWG a lift-off method is employed to pattern the gold stripes. The lift-off approach is still possible for the siloxane polymers but overall the etching process was found better than lift-off.

Our process flow is summarized in Fig. 2. In a first step, a 4-30 nm thick gold film is deposited onto the substrate, acting as an adhesion control layer needed for easy peel off the film in the end. After coating the bottom polymer cladding, a surface silane-thiol treatment is performed to enhance the adhesion of gold on the cladding. Then 15 nm gold is deposited by

Optical Materials EXPRESS

thermal evaporation. A photoresist AZ MiR 701 is coated on top of gold and structured by UV lithography with the waveguide mask. Argon sputter etching of gold is then realized in an Oxford Plasmalab 100 RIE-ICP tool. In the next step, what remains from the photoresist mask after etching is dissolved in the appropriate remover and oxygen plasma. A second surface treatment is applied to enhance the adhesion before the deposition of the top cladding. Cleaving the silicon supporting the polymer film was the simplest method we have used to obtain the coupling facets. In this process a tiny scratch is first engraved at the desired coordinate. The substrate is cleaved by applying pressure in this location but it does not break the flexible polymer at this time. The fracture of the polymer is then obtained by bending the two silicon parts at an acute angle which eventually achieves breaking the polymer film apart. This is eased by the fact that the polymer adheres well to the silicon and is held tightly during this process. The drawback of this method is that the fracture line in the polymer does not follow exactly the fracture line of the silicon and that the gold stripes might be damaged close to the fracture. This is why dicing is recommended in order to get perpendicular facet aligned with the Si fracture plane. In the final step the flexible plasmonic arc is obtained by detaching the film from the substrate, without affecting its integrity due to the gold layer atop the silicon.

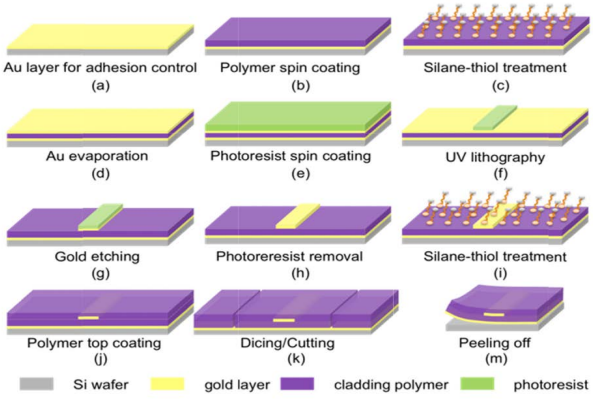

Fig. 2. Fabrication process flow based on gold etching with drawing of the silane-thiol link on gold and cladding material (silicone).

In the initial tests done without silane treatment, plasmon propagation was rather poor and hardly reproducible. This was due to air gaps trapped at the gold/polymer interfaces resulting from poor adherence between these two materials. Gaps induce a loss of symmetry of refractive index around the gold strip that is detrimental to plasmon propagation. To avoid this we introduced the two additional surface functionalization steps, one immediately prior to Au evaporation and the other one immediately before coating the top cladding. The functionalization process developed consists of a surface activation step with oxygen plasma followed by spin-coating a solution of a bifunctional molecular linker, namely 3-mercaptopropyltrimethoxysilane (3-MPS), a molecule with a silane group to anchor to Si-containing materials and a thiol group prone to bind to gold atoms. The product used was either 3-MPS purchased from Sigma-Aldrich or A-Link^{TM} 189 silane from Momentive, dissolved in absolute ethanol at 1 mM concentration. Samples are then baked at 110 °C on a hotplate to finalize the bonding. This achieves a resistant and stable linkage between the polymer matrix and the gold surface atoms. Samples fabricated with chemical functionalization steps present a plasmon mode of much better shape and size, have lower optical losses and show more reproducibility. The absence of air gaps is confirmed by SEM imaging (Fig. 3).

Optical Materials EXPRESS

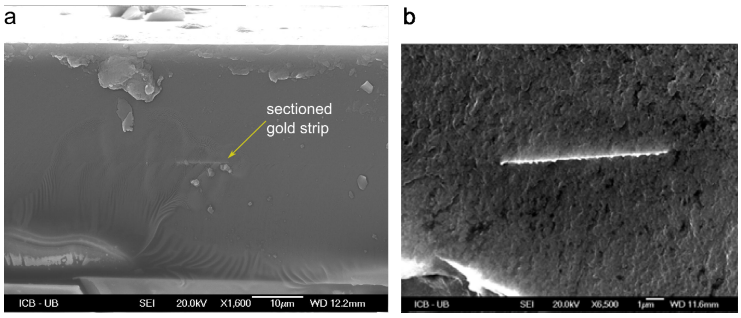

Fig. 3. (a) SEM image of the cleaved facet of the Plasmonic Arc (Momentive cladding material and 15 nm thick gold strip). (b) Enlarged SEM image. The edge of the cut strip appears irregular as a result of tearing during cleaving.

The molecular linker approach (silanization) used successfully for the siloxane-containing MPM526A&B blends and LightLink polymer does not work with FOWG, due to the fact that the silane process is not compatible with the lift-off process and that only a lift-off process was appropriate for FOWG films. Therefore, only the results of the first two materials are presented in the following.

The fabrication method was also extended to the multiple cladding configurations without major modifications of the process flow. We fabricated core and cladding plasmonic arcs by using different blends the MPM526A&B materials to obtain the different refractive index desired for each layer. The spin coating speed of the material mixtures were adjusted in order to get ~20 μm thickness for the outer cladding and ~4μm for the two layers constituting the ~8 μm thick core that is embedding the gold strip. More details of the fabricated samples are presented in section 7.

5. Losses of the standalone waveguides

To excite the LRSPP mode, we inject light at 1.55 μm from an ASE source through a single-mode fiber (SMF-28) into the waveguides by end-fire coupling, with the input power of 1-5 mW (Fig. 1(c)). The polarization was varied from TM to TE to check the SPP mode being switched on (TM) and off (TE). In our coupling approach, usually only the fundamental mode (noted as ss_b^0 according to [3]) is significantly excited due to its similar field distribution shape as the Gaussian-like input beams (in fiber or free space), and the other modes are excited with very low efficiency. An IR camera equipped with objectives was used to observe the plasmon mode in the far field, either from above the sample or from the side. Imaging with the camera enabled us to properly align the fiber with the waveguide. A single-mode output fiber attached to a power-meter was used to measure the losses. The attenuation of the plasmon propagating along the waveguide can be observed due to the radiative losses and image analysis provides an estimated propagation length. To measure the mode intensity distribution at the output facet the angle of observation is rotated by 90° with the help of a mirror as depicted in the schematics of our setup in Fig. 4(b). The field distributions we observe have typical width in the 5—15 μm range. Given the numerical aperture NA = 0.35 of our long working distance objective, these field distributions are not expected to be significantly impacted by the point spread function of our imaging setup. Consequently the raw experimental intensity distribution can be confidently compared to the computed near-field distributions [38]. Figure 4(a) compares the computed distributions with the captured IR images of the MPM526A&B LRSPPW modes of varied waveguide widths, showing a good agreement. The 100 μm pitch is large enough to avoid any cross-talk between adjacent waveguides. Similar results are obtained with LightLink material.

Optical Materials EXPRESS

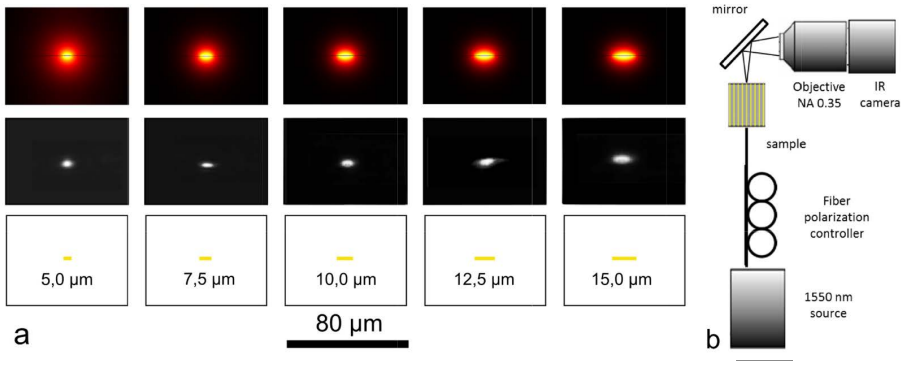

Fig. 4. (a) Images of calculated electric field distributions (top row) and captured IR images (middle row) of the Au-MPM526A&B LRSPPW modes at the output end of the waveguide for varied strip widths. (b) Optical setup used to acquire the field distributions.

The images give us the mode size in both longitudinal (along y axis) and transversal direction (along z axis) for both TE and TM polarization. Experimental and computed mode size values are reported in Table 2 and Table 3. For Lightlink, simulations find only the ss_b^0 fundamental mode for strip width smaller than 12.5 µm so that the cut-off width lies between 12.5 and 15µm. For MPM526A&B, the cut-off width is larger than 15 µm. We also remind that in our coupling scheme, higher order modes are coupled with lower efficiency than the fundamental mode and are not detected.

Table 2. Effective indices and SPP propagation length obtained from simulation. Comparison of longitudinal and transversal mode sizes (Full width at half maximum) between simulations and experiments with Au-MPM526A&B LRSPPW.

width (µm)	n_{eff}	k_{eff}	L_{SPP} (mm)	**long. mode** FWHM (µm)		**Trans. mode** FWHM (µm)	
				simulation	experiment	simulation	experiment
5.0	1.4101	$3.30e^{-6}$	37.3	8	8.7	7	5.8
7.5	1.4103	$6.89e^{-6}$	17.9	9	9.7	6	5.1
10.0	1.4105	$8.97e^{-6}$	13.7	10	11.6	6	4.8

Table 3. Experimental plasmon mode size (FWHM) at waveguide output end on 12mm long Au-MPM526A&B LRSPPW sample.

Gold strip width (µm)		**5**	**7.5**	**10**	**12.5**	**15**
MPM526A&B	Longitudinal FWHM (µm)	8.7	9.7	11.6	12.8	15.6
	Transversal FWHM (µm)	5.8	5.1	4.8	4.7	4.9
LightLink	Longitudinal FWHM (µm)	5.6	5.7	7.2	8.7	9.1
	Transversal FWHM (µm)	4.8	4.8	4.8	4.8	4.8

For loss measurement a single-mode fiber is coupled at the output end of the waveguides in place of the objective and IR camera. We scanned each sample to measure average insertion loss values from at least 5 identical waveguides in each array. There are arrays for different strip widths (5, 7.5, 10, 12.5, 15 µm). Figure 5 reveals a typical TM/TE polarization extinction ratio of about 25 dB in the case of Lightlink polymer, which is pretty satisfactory. The same polarization ratios are obtained with the Momentive blends, within the error margin.

Optical Materials EXPRESS

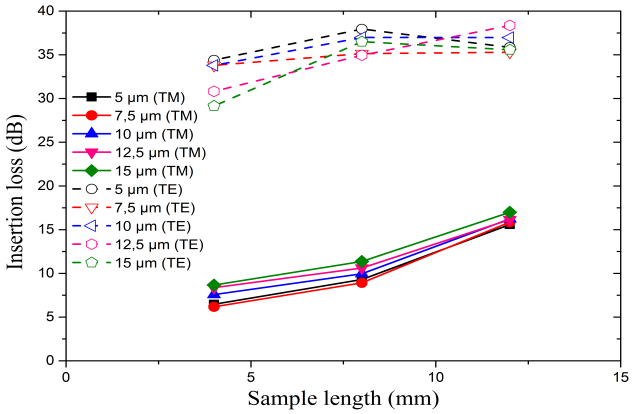

Fig. 5. Loss measurements in TM and TE polarization (Au-Lightlink LRSPPW)

The cut-back method allows us to deduce the propagation and coupling losses out of the data. The insertion losses of the TM plasmon mode are plotted in Fig. 6 for Momentive material and Fig. 7 for Lightlink material for varied waveguide widths. In both cases the propagation loss lies in the 0.3 to 1.2 dB/mm range and the coupling loss between 3 and 10 dB (for input + output facets) when normal wafer cleaving is used. The dip at about 10µm in the propagation length plot (Fig. 6(b)) might be explained by the occurrence of additional modes above this threshold. In the case of Lightlink polymer the behavior is different with little loss variation in function of waveguide width (Fig. 7). In comparison the performance of the FOWG plasmonic arcs fabricated was much poorer, with a propagation loss of ~32 dB/cm. We explain this by a symmetry break in the claddings index due to the presence of air gaps around the gold strip, as mentioned in section 4.

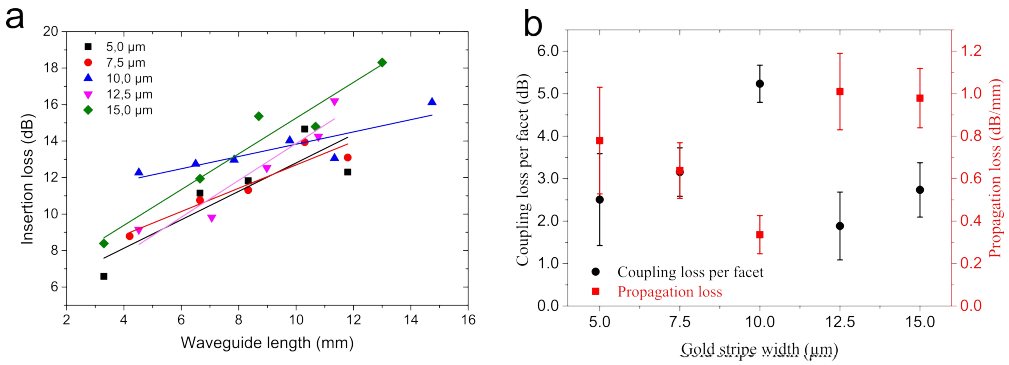

Fig. 6. Measured insertion loss of the Au-MPM526A&B plasmonic arcs versus waveguide length for gold strip widths 5, 7.5, 10, 12.5 and 15 µm. The coupling facets were obtained by cleaving. Straight lines are linear fits of the measurements. (b) Calculated coupling loss and propagation loss with error bar by cutting-back method with the data from (a)

Optical Materials EXPRESS

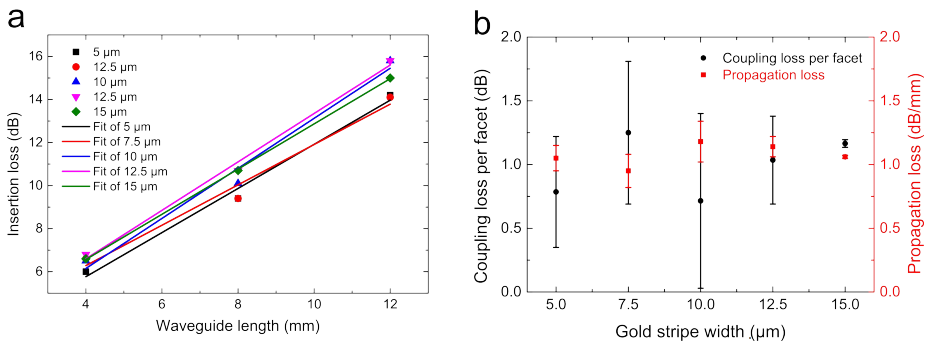

Fig. 7. Measured insertion loss of the Au Lightlink plasmonic arcs versus waveguide length for gold strip widths 5, 7.5, 10, 12.5 and 15 μm. The coupling facets were obtained by dicing. Straight lines are linear fits of the measurements. (b) Calculated coupling loss and propagation loss with error bar by cutting-back method with the data from (a).

The quick and easy cleaving method usually resulted in a variable coupling loss between 3 and 10 dB depending on the waveguide (Fig. 6). To improve this, test wafers were cut with a dicing saw. As a result, the coupling loss was slightly decreased to the 3-6 dB range, thus not in a significant manner but with less variance (Fig. 7). The differences in coupling loss observed between the two materials are attributed to the different cutting methods used in the two cases but not to materials.

6. Bending loss measurement of single cladding plasmonic arcs

We present the characterization results of the curved single-cladding plasmonic arcs fabricated with Lightlink material (n = 1.476). The plasmonic arcs are peeled off from the silicon wafer to measure the bending loss. Two experimental setups were used: firstly a single S-bend with fixed bending radius and secondly a double S-bend configuration where both ends of the samples were fixed to movable stages, with the middle part of the waveguide suspended in air. In the latter case different radii of curvature could be reached by decreasing the distance between the two stages. Both methods gave similar results: the bending loss of plasmonic arc with 7.5-μm-wide gold stripe is about 2.2-2.8 dB/90°, and the polarization ratio is 15-20 dB for a bending radius r of 2.5 mm. The double-bend and the corresponding loss plot are shown in Fig. 8. After the LRSPP mode is excited by an SM fiber from one end, the maximum output intensity is obtained from the other end. The stage with the output end of the sample is moved towards the input end to bend the middle part of the waveguide. In this case, the fluctuation of the coupling efficiency in the input end is minimized. In order to obtain the bending radius value, we assume the bending part of the waveguide is composed of four identical parts of arc, with the same radius r and bending angle θ, as shown in Fig. 8(b). The length of the bending part of the waveguide is l, and the decreased length d. The bending radius can be determined easily from the two equations $4r\theta = l$ and $4r\sin\theta = l - d$.

Optical Materials EXPRESS

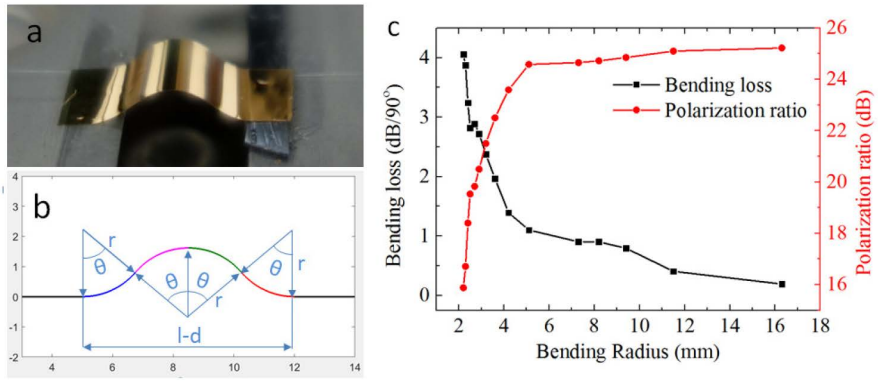

Fig. 8. (a) Photograph of the bended plasmonic arc with both ends attached to narrow silicon stripes. (b) Curve model for the calculation of the bending radius. (c) Measured bending loss and polarization ratio versus bending radius for w_{strip} = 7.5 μm.

The total length of the flexible arc is 12 mm and l is 8 mm. By moving the two stages, the bending radius decreases from 16.3 to 2.2 mm. The measured bending loss and polarization ratio for the 7.5-μm-wide gold strip are shown in Fig. 8(c). A high polarization ratio (from 25 to 16 dB) is maintained even when r decreases to 2.2 mm. The bending loss is slowly increasing when r drops from 16.3 to 5 mm (from 0.2 to 1.1 dB/90°), and then fast with further decreased bending radius (4 dB/90° at r = 2.2 mm). The bending loss and polarization ratio are 2.8 dB/90° and 20 dB at r = 2.5 mm, respectively, which are pretty close to the counterpart result (2.2 dB/90° and 15 dB) of S-bend configuration with the same radius. The slightly increasing bending loss indicates that the sample suffers little deterioration even after it has been curved in the S-bend configuration, demonstrating the flexibility and stability of the waveguide.

7. Bending loss measurement of double-cladding plasmonic arcs

Double-cladding plasmonic arcs show reduced bending loss compared to the single-cladding ones. The structure studied is illustrated in Fig. 9(a). Two blends I and II were made from the provided MPM526A&B materials in different proportions to generate both inner and outer claddings with refractive indices of 1.468 and 1.458, respectively. The thicknesses of the inner and outer claddings are 4-6 and 10-20 μm, respectively. The electric field of the LRSPP mode is mainly confined in the inner cladding layers around the gold stripe, as shown in Fig. 9(b), obtained by a finite-element numerical method.

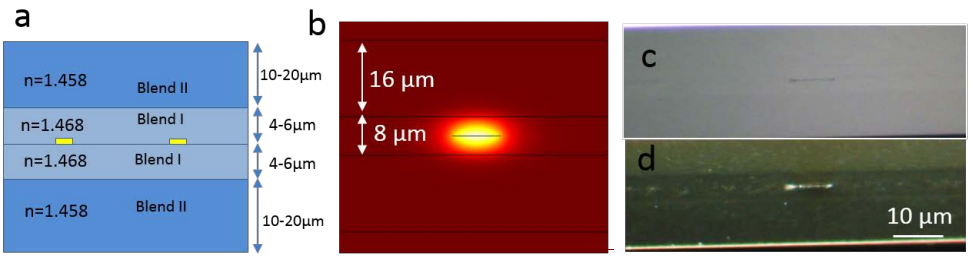

Fig. 9. (a) Structure layout of the double-cladding plasmonic arc. (b) Calculated electric field distribution of the fundamental TM mode with gold w = 10 μm and t = 15 nm. Optical microscope images from side view in bright (b) and dark (c) field.

The insertion loss and polarization ratio of the straight plasmonic arc are measured both before and after separation from the substrate. The results in Table 4 show that the damage is

Optical Materials EXPRESS

avoided pretty well with a careful peeling process even though the gold underlayer is only 4 nm thick in this sample: the insertion loss of the 11-mm long arc has increased by 0-2 dB, and the polarization ratio is also still larger than 20 dB. Since the coupling loss is always 1-2 dB/facet, the propagation loss of the straight plasmonic arc is about 1.2-1.5 dB/mm, which is close to the values obtained in other plasmonic arc samples.

Table 4. Comparison of insertion loss and polarization ratio of the straight double-cladding plasmonic arc of different gold strip widths before and after being peeled off from the silicon wafer.

	Insertion loss (dB) / Polarization ratio (dB)		
Gold strip width	7.5 μm	10 μm	12.5 μm
Before peeling off	17/21	17/26	16/24
After peeling off	19/20	17/23	17/24

Bending loss was measured in the varying bending radius configuration as in the previous section. When the incident light is TE polarized or the light is coupled to the polymer layers above or below the gold strip, the incident light will not be coupled into well-confined mode, only diffusing and dissipating into the polymer. The length of the cleaved sample is 11 mm, but the length of the bendable part of the flexible waveguide is between 5, 7 and 8 mm. Generally speaking, the performance of this double-cladding sample presented in Fig. 10 has much improved compared to that of the single-cladding one. The bending losses at r = 2.5 mm for 5-, 10- and 12-μm gold stripes are 1.5, 1.7 and 0.7 (and 1.2 for 12.5 μm B) dB/90°, compared to 2.2-2.8 dB/90° for the single cladding case. The bending loss increases much for bending radii smaller than 2 mm (3 mm for the case of 10 μm-wide strip). Similarly, the polarization ratio is maintained above 10 dB for bending radii larger than ~2 mm (Fig. 10(c)). The observed fluctuations of the polarization ratio may relate to the instability of the polarization controller. Therefore, the low polarization ratio of the incident wave could lead to degraded performance of the plasmonic arc.

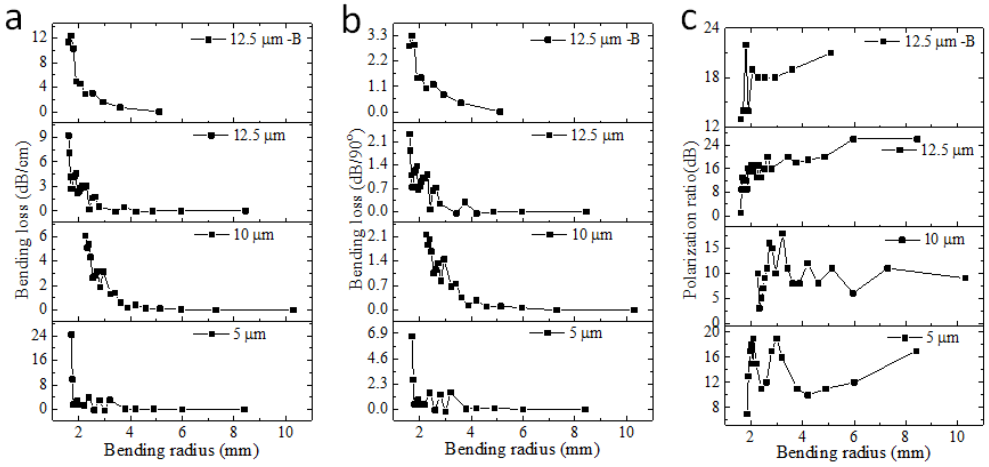

Fig. 10. Double-cladding plasmonic arc: measured bending loss of the LRSPP mode by dB/cm (a) by dB/90°, (b) and polarization ratio (c) versus bending radius of arc with the gold strip width of 5, 10, and 12.5 μm respectively. "12.5 μm B" indicates another waveguide with gold stripe width of 12.5 μm but different length in the same sample.

The double-cladding structures therefore experiences very low bending loss when r>2 mm (<2 dB/90° at r = 2.5 mm), which is slightly better than the single-cladding one. We did additional tests to study the ability of the samples to recover their original state after bending. The free-standing plasmonic arcs were wrapped by 180° around some cylindrical pillars with radius between 0.5 and 3 mm. We observe that, even when the bending radius reaches 1.5

Optical Materials EXPRESS

mm, the samples relax to their original state without residual damage. Only after the bending radius is smaller than 1.5 mm, some extra small cracks of the gold strip can be detected under optical microscope with the polymer still intact. The waveguides do not break even when the bending radius reaches 0.5 mm. The results demonstrate that plasmonic arcs have excellent flexibility and stability under bending circumstances.

8. Coupling of the plasmonic arc with single-mode ion-exchanged glass waveguides

We finally report on the optical coupling of the plasmonic arcs with single-mode glass waveguides, which can be used as optical printed circuit board (OPCB). This is the first step towards the commercial application of plasmonic arcs as interconnects. The fabrication process and performances of the glass waveguides have been described elsewhere [39,40]. The glass waveguide samples used show very low propagation loss, below 0.015 dB/mm. The Measurement Identification Code of our interfacing experiment according to IEC 62496-2 standard was MIC 141-011-011-011-011. Using SM fibers and a 1.55 µm source, the insertion loss is 2.2 dB for a 31 mm long sample. The glass waveguides used were in an early production stage, thus showing varying propagation losses of 0.005-0.015 dB/mm and fiber coupling losses of 0.6-1.6 dB/facet. These measurements were performed by an additional cutback measurement.

The 31 mm long glass waveguide and input fiber were aligned first by observing the output mode on the IR camera placed in the axis of propagation. The FWHMs of the mode were measured to be 11.5 µm in both longitudinal and transversal directions. Then an 8 mm long plasmonic arc sample was aligned with the glass waveguide output by optimizing the output mode imaged at the ending facet. Finally the output fiber was aligned by optimizing the readout of a power-meter. While the standalone plasmonic arc and the glass waveguide feature an insertion loss of ~12 dB (+/–0.5 dB depending on strip width) and 2.2 dB respectively, the insertion losses measured for the glass plus plasmonic arc couple are ranging between 13—16 dB for TM polarization (see Table 5) and 35—37 dB in TE, depending on the plasmonic strip width W_{strip}. It was also checked that the values were the same when the two samples were inverted with respect to the propagation direction.

Table 5. Coupled OPCB / Plasmonic Arc insertion losses (TM polarization)

	Plasmonic Arc strip width	5µm	7.5µm	10µm	12.5µm	15µm
Insertion Loss in TM (dB)	Standalone PlasArc	12.6	12.6	12.2	11.8	11.5
	Standalone OPCB			2.2		
	OPCB->PlasArc	16.0	13.6	13.3	13.1	12.8

The plasmonic arc to glass waveguide coupling loss $C_{\text{Arc-OPCB}}$ was deduced by the following calculation where we define $C_{\text{fiber-Arc}}$ and $C_{\text{fiber-OPCB}}$ as the fiber coupling losses involved, P_{Arc} and P_{OPCB} as the propagation losses obtained from the cutback studies and L_{Arc} and L_{OPCB} the lengths of the samples. Equation (1) gives the total insertion loss of the OPCB-arc assembly:

$$Loss = C_{fiber-arc}\left(W_{strip}\right) + L_{arc}P_{arc}\left(W_{strip}\right) + C_{arc-OPCB}\left(W_{strip}\right) + L_{OPCB}P_{OPCB} + C_{fiber-OPCB} \quad (1)$$

where $L_{OPCB}P_{OPCB}$ = 0.015x31 dB and L_{arc} = 8 mm. $C_{\text{fiber-OPCB}}$ is deduced from the insertion loss I_{OPCB} = 2.2 dB of the standalone OPCB waveguide and P_{OPCB} by the following equation:

$$C_{fiber-OPCB} = \left(I_{OPCB} - L_{OPCB}P_{OPCB}\right)/2 \quad (2)$$

The results are presented in Fig. 11. We observe that the insertion loss tend to decrease as a function of W_{strip}. The 10 µm width seems to be the optimum for the coupling at the interface

Optical Materials EXPRESS

between the two elements but 12.5 and 15µm are pretty close and the relatively small difference between the 3 values of W_{strip} could be due to the local variations of the coupling loss $C_{fiber\text{-}Arc}$ linked with the quality of the cleaving. The noticeable decreasing trend between 5 and 10 µm is more important and is certainly due to increased mode size mismatch. The coupling loss of 1.7—2.3 dB/interface with the gold strip widths equal to or larger than 10 µm is decent performance for plasmonic arc interconnects.

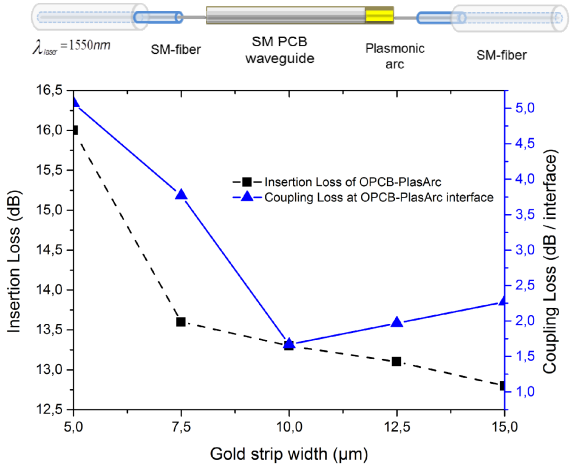

Fig. 11. Optical losses of the OPCB-Plasmonic Arc assembly. The lengths of the OPCB waveguide and plasmonic waveguide are 61 mm and 8 mm, respectively.

9. Conclusions

We selected materials MPM526A&B and LightLink as suitable polymer materials for flexible free-standing LRSPP waveguides (plasmonic arcs) with gold as the plasmonic metal. We have developed a fabrication method based on etching of gold and using a covalent surface modification of gold to promote adhesion to the polymer claddings, a necessary condition to assure good propagation length. Both materials gave plasmonic arcs with similar optical performances at 1.55 µm, with a propagation loss most often below 1 dB/mm in TM polarization and ~25 dB TM/TE polarization ratio in the straight configuration. The performances were slightly better for Momentive materials with a minimum of ~0.3 dB/mm for a gold strip width of 10 µm. The coupling losses reached about 1 dB/facet after dicing. In the free-standing S-curved configuration, the bending loss of single cladding plasmonic arc was 2.2-2.8 dB/90° at bending radius 2.5 mm. For double cladding plasmonic arcs, it decreased to 0.7-1.7 dB/90° for the same radius. The coupling loss with glass waveguide OPCB estimated to 1.7 dB in the best condition proved the potentiality of plasmonic arcs to act as single mode high-density on-board interconnects for data center, HPC or other applications.

Funding

European Commission through the FP7 ICT grant n° 318240 (project PhoxTroT) and grant n° 287874 (project FIREFLY, which is acknowledged for the research leading to Momentive's material development).

Acknowledgments

We acknowledge TE Connectivity, in particular J. Duis and S. Dorrestein for the dicing work. Momentive acknowledges the continuous support from TNO Eindhoven (NL), especially from S. Wiegersma, N. Meulendijks and A. Boersma. The "Centre de Ressources

Optical Materials EXPRESS

Mécaniques" of the ICB laboratory in Dijon is acknowledged for contributing to the development of an optical characterization setup.